Received: 18 March 2020 | Revised: 18 May 2020 | Accepted: 20 May 2020

DOI: 10.1096/fj.202000629R

RESEARCH ARTICLE

THE FASEB JOURNAL

Resident mesenchymal vascular progenitors modulate adaptive angiogenesis and pulmonary remodeling via regulation of canonical Wnt signaling

Megan E. Summers[1] | Bradley W. Richmond[2] | Swapna Menon[3] | Ryan M. Sheridan[4] | Jonathan A. Kropski[2] | Sarah A. Majka[1] | M. Mark Taketo[5] | Julie A. Bastarache[2] | James D. West[2] | Stijn De Langhe[6] | Patrick Geraghty[7] | Dwight J. Klemm[8,9] | Hong Wei Chu[1] | Rachel S. Friedman[10] | Yuankai K. Tao[3] | Robert F. Foronjy[7] | Susan M. Majka[1,9,10,11]

[1]Department of Medicine, Division of Pulmonary, Critical Care & Sleep Medicine, National Jewish Health, Denver, CO, USA

[2]Department of Medicine, Division of Allergy, Pulmonary and Critical Care Medicine or Cardiology, Vanderbilt University Medical Center, Nashville, TN, USA

[3]Pulmonary Vascular Research Institute Kochi, AnalyzeDat Consulting Services, Ernakulam, India

[4]Department of Biochemistry and Molecular Genetics, RNA Bioscience Initiative, University of Colorado School of Medicine, Aurora, CO, USA

[5]Division of Experimental Therapeutics, Graduate School of Medicine, Kyoto University, Kyoto, Japan

[6]Department of Medicine, University of Alabama, Birmingham, AL, USA

[7]Division of Pulmonary and Critical Care Medicine, SUNY Downstate Medical Center, Brooklyn, NY, USA

[8]Department of Medicine, Pulmonary & Critical Care Medicine, University of Colorado, Aurora, CO, USA

[9]Gates Center for Regenerative Medicine and Stem Cell Biology, University of Colorado, Aurora, CO, USA

[10]Department of Biomedical Research, National Jewish Health, Denver, CO, USA

[11]Biomedical Engineering, Vanderbilt University, Nashville, TN, USA

Correspondence
Susan M. Majka, Department of Medicine, Division of Pulmonary, Critical Care & Sleep Medicine, National Jewish Health, 1400 Jackson St, K810, Denver CO, 80206, USA.
Email: susanmajka@mac.com

Funding information
This work was funded by grants to SM Majka from the NIH R01HL116597 and NIH R01HL136449. The project was also supported in part by the National Center for Research Resources, Grant UL1 RR024975-01 and is now at the National Center for

Abstract

Adaptive angiogenesis is necessary for tissue repair, however, it may also be associated with the exacerbation of injury and development of chronic disease. In these studies, we demonstrate that lung mesenchymal vascular progenitor cells (MVPC) modulate adaptive angiogenesis via lineage trace, depletion of MVPC, and modulation of β-catenin expression. Single cell sequencing confirmed MVPC as multipotential vascular progenitors, thus, genetic depletion resulted in alveolar simplification with reduced adaptive angiogenesis. Following vascular endothelial injury, Wnt activation in MVPC was sufficient to elicit an emphysema-like phenotype characterized by increased MLI, fibrosis, and MVPC driven adaptive angiogenesis. Lastly, activation

Abbreviations: Abcg2, ATP-binding cassette super-family G member 2; CSE, cigarette smoke exposure; MDR, multidrug resistance; MVPC, Mesenchymal vascular progenitor cells; PH, pulmonary hypertension; RA, room air; Sugen, receptor tyrosine kinase inhibitor, SU5416; VEGF, vascular endothelial growth factor; WT, wild-type; βOE, stabilized β-catenin.

Advancing Translational Sciences, Grant 2 UL1 TR000445-06. Experiments were performed using the University of Colorado Cancer Center Microarray Core (NCI P30 CA 46934-14) and Shared Flow Cytometry Resource (P30-CA046934 NCI).

of Wnt/β-catenin signaling skewed the profile of human and murine MVPC toward an adaptive phenotype. These data suggest that lung MVPC drive angiogenesis in response to injury and regulate the microvascular niche as well as subsequent distal lung tissue architecture via Wnt signaling.

KEYWORDS

adaptive angiogenesis, emphysema, mesenchymal vascular progenitor cell, microvascular niche, Wnt signaling

1 | INTRODUCTION

Loss and dysfunction of pulmonary microvasculature has been implicated in the decreased alveolar gas exchange area in emphysema, a major manifestation of chronic obstructive pulmonary disease (COPD). Recent evidence highlighted a role for microvascular pathology in both the early pathogenesis and heterogeneity of the disease.[1-5] However, the mechanisms by which changes in the microvasculature underlie the development of chronic lung diseases remain unresolved. To date, studies have primarily focused on endothelial cell injury as the basis for microvascular dysfunction during the development of emphysema, while lung resident mesenchymal cell types and adaptive angiogenesis have been largely overlooked. We, therefore, tested the hypothesis that lung mesenchymal vascular progenitor cells (MVPC) modulate adaptive angiogenesis and pulmonary tissue remodeling via regulation of canonical Wnt/β-catenin signaling. MVPC may, therefore, contribute to the development of emphysema by altering the homeostatic maintenance of the microvascular niche.

Adaptive angiogenesis occurs in response to tissue hypoxia, injury, and during wound healing. However, this de novo angiogenesis, while reparative in nature, can also become maladaptive if not patterned correctly via remodeling, regression, and pruning.[6-8] Mesenchymal regulation of pulmonary vasculogenesis and angiogenesis in the distal lung have been well-characterized during development.[9-11] Recently, lineage analysis using a lung-specific enhancer coupled to the mesenchymal restricted transcription factor Tbx4 provided evidence for mesenchymal-derived angiogenic precursors.[12,13] MVPC have since been lineage labeled and characterized in adult murine lung during both tissue homeostasis and disease.[14-17] Their perivascular localization and communication[14,18] would predict crosstalk between MVPC and components of the lung microvasculature during health and distal lung injury resulting in emphysema.

In this report, using murine and human models, we described a vital role of resident lung MVPC as multipotent vascular progenitors in maintaining the integrity of the distal lung during homeostasis and adaptive angiogenesis in response to injury. These studies also defined how disease specific increases in canonical Wnt/β-catenin signaling by MVPC influenced adaptive angiogenesis within the lung microvascular niche.

2 | MATERIALS AND METHODS

2.1 | Study approval

The Institutional Animal Care and Use Committee at National Jewish Health or Vanderbilt University approved all animal procedures and protocols. These studies utilized banked patient cell lines obtained using IRB #9401 approved by the Vanderbilt University Medical Center IRB Committee, Nashville, TN, USA. Patients were consented under this IRB for the generation and storage of human cell lines. Primary cells were obtained from advanced COPD patients (GOLD C or D) with severe physiological impairment (FEV1/FVC < 0.7 and FEV1% Pred < 30%) requiring lung transplantation as previously described.[14,19]

2.2 | Study design

Isolated human and murine MVPC and murine in vivo age matched models were utilized. Endpoint analysis was performed in a blinded fashion. Sample size and number of replicates are specified in the figure legends, methods, and Supporting Table S1. We have previously reported that the recombination efficiency, at two alleles, is approximately 50%[14] and that recombination with GFP expression strongly correlated with Abcg2 (Supporting Figure S2B-F).

2.2.1 | Isolation and characterization of primary lung MVPC

Human lung plastic adherent cells were isolated from explant lung tissue post autopsy or transplant by collagenase digest (Vanderbilt IRB Protocol 9401) to form a suspension. The cells were stained with antibodies to sort $CD45^{neg}$ $ABCG2^{pos}$ cells (lung mesenchymal progenitors) using a

BD FACSAria III (BD Biosciences, San Jose, California). Techniques were previously described and ABCG2 was validated as a cell surface marker for both murine eGFP labeled and human MVPC.[14,18] Antibodies for flow cytometry were purchased form eBiosciences, (San Diego, CA) or Thermo Fisher (Waltham, MA). A summary of human lung mesenchymal progenitor line expression of cell surface determinants is presented in Supporting Tables S3 and S4.

Murine lung mesenchymal progenitors were isolated from induced ABCG2 Cre^{ERT2} × mT/mG mice using a BD FACSAria III (BD Biosciences, San Jose, California) to identify eGFP positive cells. Isolated cells were plated on attachment factor-coated dishes, expanded, and analyzed at passage 7 to characterize CFUF and cell surface determinants as previously described.[14,18] Following expansion, all primary human and murine mesenchymal progenitors were analyzed by flow cytometry to confirm the presence of CD105, CD106, CD73, ScaI, CD44 and the absence of c-kit, CD14, and CD45 (Supporting Table S4) using a BD Fortessa or LSRII (BD Biosciences, San Jose, California). Following cell sorting, $CD45^{neg}$ GFP^{neg} or $CD45^{neg}GFP^{pos}$ populations were centrifuged to make cytospins for analysis (Wescor Cytopro). To compare relative growth characteristics of mesenchymal progenitors and colony forming unit-fibroblast colonies (CFU-F), cells were counted and diluted to a concentration of 6×10^3/mL. After colonies were formed, spent medium was removed and cells washed once with DPBS. About 4% of paraformaldehyde was used to fix the cells for 20 minutes. Following a PBS wash, Giemsa stain (Sigma Aldrich, Saint Louis, MO; Cat# GS500) was added to cover cells overnight. Giemsa stain was then removed, and the plates gently washed with water (Supporting Figure S5E).

2.2.2 | Genetic manipulation of murine $ABCG2^{pos}$ mesenchymal progenitor cells (MVPCs)

ABCG2-Cre^{ERT2} mice, a generous gift of Dr B. Sorrentino (St. Jude Children's Research Hospital, Memphis, TN),[20] were crossed to a fluorescent eGFP reporter (Cg)-Gt(ROSA)26Sortm4(ACTB-tdTomato,-EGFP) JAX stock# 007676; designated mT/mG) strain to facilitate lineage analysis and quantitation via eGFP expression. A third gene was crossed into the mice to stabilize βcatenin($Catnb^{loxp}$(Δex3) a generous gift of Dr MM Taketo (Kyoto University, Kyoto, Japan).[21] To knockout MVPC in vivo, we crossed the Abcg2 driver/reporter strain to a mouse containing a floxp stop allele regulating the expression of Diphtheria toxin A[22,23] (JAX stock# 009669). Mice were injected intraperitoneally at 8-10 weeks of age with a low dose (0.5mg) tamoxifen (T-5648; SIGMA, St. Louis MO) in sesame oil, or sesame oil alone (vehicle control).[18,24] The mice were randomized and distributed as 3-5 mice per cage for studies. These model systems, as well as isolated MVPC, were validated as previously described.[14]

2.2.3 | Phenotyping of pulmonary vascular dysfunction

Elevated pulmonary artery pressure was documented indirectly by the measurement of right ventricular systolic pressure (RVSP) as previously described.[25] RVSP was measured at the time of harvest.[25,26] The number of subjects per group was 6-8. Histologic endpoints included muscularization and microvessel density of the distal microvessels by immunostaining to detect smooth muscle actin (SMA; Dako clone 1A4) or Factor 8 (A0082 DAKO) on 6-8 mice per group.[25] The average inter-alveolar distance was assessed by quantification of MLI in lungs inflated with agarose under constant temperature and pressure as described.[27,28] H&E-stained lung sections from 6 to 8 wild-type or transgenic mice were analyzed. For each pair of lungs, 40 histological fields were photographed and evaluated in a blinded fashion. Immunofluorescent staining was performed to lineage trace eGFP-labeled lung mesenchymal progenitors and localize smooth muscle alpha (SMA), reagents outlined in Supporting Tables S6 and S7. Quasi-static mechanical properties of the lung we measured using the flexiVent invasive plethysmography system (SciREQ, Inc) as previously described.[29-31]

2.2.4 | Cigarette smoke exposure and Stereology

Mice were exposed to cigarette smoke for four hours daily, five days a week for 1 month. To expose the mice to cigarette smoke, two 70 mL puffs per minute from research cigarettes (University of Kentucky, 3R4F) were generated by a smoking machine (SIU24 system; Promech, Vintrie, Sweden), and then, diluted with fresh air and delivered to whole body exposure chambers. The mice were subjected to a mixture of both mainstream and side stream smoke. The total particulate matter (TPM) concentration in the chamber was kept at 100 mg/m^3 at all times.[32,33] The TPM was determined by gravimetric analysis of filter samples taken during smoke exposure. Blood carbon monoxide levels in these mice were below 10%. To analyze changes in distal lung structure, images of H&E stained lung sections were taken on a Nikon Eclipse 80i microscope using NIS Elements AR software (version 4.13). A minimum of 6 non-overlapping images were taken at 20x to avoid large vessels or airways. Images were then loaded into an interactive macro within Metamorph Software (version 7.5.0.0) for analysis.[32] MLI and MCL were calculated from the average of

all the images and the surface to volume ratio was calculated as 4 × Sum of line Intercepts/130.87 × Sum of ends.

2.2.5 | RNA scope

RNA scope was performed using the Advanced Diagnostics HybEZII system with the RNAscope Multiplex Fluorescent Reagent Kitv2 assay per manufacturer instructions. Probes included GFP (cat# 400281) and Abcg2 (510101).

2.2.6 | Western blot analysis

Protein extracts were made by scraping cells in RIPA buffer (Cell Signaling, Boston, MA; cat # 9806S) containing protease and phosphatase inhibitors (ThermoFisher Scientific, Waltham, MA; cat # 78444). After determination of protein concentrations and standardization, cell lysates were mixed with an equal volume of Laemmli SDS loading buffer, resolved on 10% of polyacrylamide-SDS gels, and transferred to PVD membranes. The blots were blocked with phosphate-buffered saline (PBS) containing 5% of dry milk and 0.1% of Tween 20, and then, treated with antibodies that detect the target proteins as labeled in the figures overnight at 4°C. The blots were washed and subsequently treated with appropriate secondary antibodies conjugated to horseradish peroxidase. After the blots are washed, specific immune complexes were visualized with SuperSignal West Pico Chemiluminescent Substrate (Supporting Table S7).

2.2.7 | Spheroid assay & quantitation

Confluent MVECs were serum starved with medium containing 0.5% of FBS for 1 hour, then, treated with 10 μg/mL low density lipoprotein conjugated to Alexa Fluor 594 (ThermoFisher L35353) in regular culture medium. After incubation, cells were rinsed twice with PBS before passaging for spheroid formation. A micro-mold (MicroTissues Inc #24-906) was used to create a 2% of agarose three-dimensional petri dish containing 96 individual recesses, which allow cells to self-assemble into spheroids. 3D petri dishes were pretreated with 1 mL of culture medium for 45 minutes (3 treatments of 15 min each) prior to cell seeding in a 24 well plate. MVECs were mixed at a 3:1 ratio with GFP^+ MVPCs and seeded into the 3D dish at a density of 500 cells per well in 75 μL total volume per the manufacturer's recommendation. Cells were allowed to settle for 30 minutes before adding 1 mL of medium to the area surrounding the micro-mold. Cells were then cultured for 24 hours, during which time spheroid formation was observed. Spheroids were collected by aspirating the medium surrounding the 3D petri dish, and squirting 500 μL of pre-warmed medium into the mold to dislodge spheroids. Spheroid-containing medium was collected into a 15 mL conical tube and centrifuged for 5 minutes at 110 *g*. Supernatant was aspirated, and spheroids were resuspended in a solution of 2 mg/mL rat tail collagen (Gibco A10483-01) combined with an equal volume of 0.5% 4000 cP methylcellulose solution (Sigma M0512) in medium. Spheroids were then pipetted in 1 mL volumes to a new 24 well plate and incubated for 30 minutes to polymerize the collagen before adding 100 μL of culture medium to each well. After 24 hours, spheroids were imaged on a Keyence BZ-X810 digital fluorescent microscope. BZ-X800 analysis software was used to measure the migratory radius of cells around the spheroid.

2.2.8 | Single cell RNA sequencing

Approximately 4000 ABCG2 eGFP labeled cells were captured and single-cell RNA sequencing libraries were prepared using the 10x Genomics Chromium 3′ v3 platform. Libraries were sequenced on an Illumina NovaSeq 6000 (paired-end; read 1:28 cycles, read 2:100 cycles) to an average depth of >120 000 reads per cell. RNA sequencing reads were processed and aligned to the mouse genome (mm10) using the Cell Ranger pipeline (v3.0.2) from 10x Genomics. Analysis was performed using the Loupe Cell Browser v. 3.1.1 10x Genomics.

2.2.9 | Optical coherence microscopy

A custom-built optical coherence microscopy (OCM) system was used for ex vivo imaging. A 0.2 obstruction-to-pinhole ratio (diameter-to-diameter) annular aperture was used to generate a Bessel beam to increase OCM depth-of-field. The aperture dimensions were tuned to optimize depth-of-field while minimizing complex conjugate artifacts. All images were acquired with a 0.1 NA 10x PLAN objective (Leica). Lateral resolution and depth-of-field were 1.8 and 106 μm, respectively. OCM data were collected using a custom-built spectrometer with a superluminescent diode light source (889 ± 93 nm bandwidth, Superlum) detected at 70 kHz line-rate using a 4096 pix. CMOS array (Basler). Axial resolution was 2.1 μm in air and system SNR was 94 dB with 900 μW on the sample. All volumetric data sets were acquired over a 1 × 1 mm field-of-view with 1000 × 1000 A pixels in 14.6 s. Individual OCM volumes were dispersion compensated and cropped to only retain in-focus depths. OCM images were acquired at 5 random fields in each of the nine optically cleared lungs (5 control, 4 disease). Custom MATLAB code was used to quantify en face projections of each OCM volume using OCM contrast as a surrogate for vasculature. The images

were first binarized using a threshold set 5 times above the standard deviation of the noise floor. Microvascular regions were then manually segmented and total vascular density in each region was calculated as the ratio between total pixels with and without signal. One-sided two-sample *t* test of unequal variances shows statistically significant differences in mean vascular density between control and disease animals ($P < .005$, alpha = 0.05).

2.2.10 | Electrical cell-substrate impedance sensing (ECIS)

Human lung MVECs (Lonza, Walkersville) were plated at a concentration of 112 500 cells per well on gelatin coated 8W1E PET ECIS culture ware arrays (Applied Biophysics, Troy) overnight to achieve confluence. The following day, MVPCs were added at a concentration of 37 500 cells per well. Prior to experiments the optimal concentration of MVEC and ratio of MVPC was determined. MVPC lines were normalized by cell number. Controls for these experiments included untreated MVEC and MVEC with wounding. On the third day, the arrays were put on the ECIS ZTheta, Applied Biophysics (Troy, NY). Resistance recordings were performed at 4 kHz every 10 minutes over 24 hours. At 2-3 hours, an electrical wound was created by administering a 20 second pulse at 60 000 Hz. In some cases, the pulse was immediately repeated to ensure cell death. In other experiments not including MVPC, a total 150 000 MVEC were applied per well and allowed to adhere overnight. Recovery from wounding in all experiments was normalized to the first resistance value data collected subsequent to wounding. These experiments were performed with two sample replicates and repeated twice.

2.2.11 | Transcriptome analysis

Array analysis and qRT-PCR was performed as described,[24,26] in triplicate or with an n of three or greater independent patient samples. Briefly, total RNA was prepared with Qiagen RNA Isolation Kit reagents (Qiagen, Valencia, CA) for total RNA isolation and analysis of gene expression. qRT-PCR assays were performed in triplicate and levels of analyzed genes were normalized to hypoxanthine phosphoribosyltransferase abundance (GAPDH or HPRT; primer list is provided in Supporting Table S6). Complimentary DNA generated from amplified RNA was hybridized to duplicate Affymetrix (Santa Clara, CA) Human Gene 1.0 ST arrays. Microarray analysis was carried out using Bioconductor version 3.2 (R 3.2.2). The oligo package was used to read in and normalized the data with RMA. The moderated *t* test implemented in the limma package was used for differential expression testing. Genes that were significantly upregulated or downregulated ($P < .05$) and showed an expression fold change of at least 1.7-fold greater or lesser than control samples were used for further analyses. Normalized expression values for these genes are represented in a heatmap. Further, the corresponding gene names were queried against the STRING database (http://string-db.org/, accessed December 10, 2015) to explore the protein-protein interactions. PathVisio 3.2.1. was used to schematically represent and annotate the relevant functional association network of differentially expressed genes. The raw array data and normalized matrix is available under the GEO accession GSE94060.

2.2.12 | Quantitation of collagen

About 10 fields of view per two sections, four sections per mouse of trichrome stained mouse lungs were photographed at 20x-40x mag. Resulting color images were scanned to quantitate the number and intensity of blue (collagen) positive pixels relative to red. n = 7-8 per group. Images were scanned using Fiji (Image J; version 2.0.0-rc-43/1.51a) using a custom plug in written by M. Majka (Denver, CO). The tool was written in the ImageJ macro language to detect pixels with a blue intensity over a desired threshold. This macro set all pixels that had the desired blue intensity to the color yellow and outputs a count of the number of yellow pixels. The specified threshold limit was based on a positive and negative control image.

2.2.13 | Imaging

Epifluorescent and brightfield images were captured with Nikon Eclipse 90i upright epifluorescence or Nikon Eclipse TS100 using the Nikon DS-Fi1 camera with NIS elements AR 4.11.00 acquisition software. The BZ-X800 KEYENCE system, with capture and analysis software, was also used. Two photon imaging was performed as previously described.[34] Fluorochromes used included DAPI (to label nuclei), secondary antibodies conjugated to Alexa 488 or Alexa 594 (ThermoFisher, Hampton, NH) to detect antibodies outlined in Supporting Table S7.

2.3 | Statistical analysis

Data were analyzed by one-way ANOVA followed by Tukey's HSD post-hoc analysis. Murine qPCR and patient samples were analyzed using nonparametric Wilcoxon/Kruskal Wallis and a chi square approximation. All analyses used JMP version 9.0.2. Data presented as ± standard error from the mean (±SEM). Significance was defined as *P*-value <.05*, *P*-value <.01** or *P*-value <.001***.

3 | RESULTS

3.1 | MVPC are an essential constituent of distal lung tissue structure

Abcg2, the multidrug resistance (MDR) transporter largely responsible for the side population (SP) phenotype of cells, has been used by our group and others to enrich for putative progenitor cells in many adult tissues in various species.[14,18,20,35-40] To localize the lineage labeled MVPC in the three-dimensional tissue structure, precision-cut lung slices (PCLS) were imaged using two-photon microscopy (Figure 1A-C). The imaging depicts that MVPC have multiple long processes in the alveolar-capillary regions (LINK to

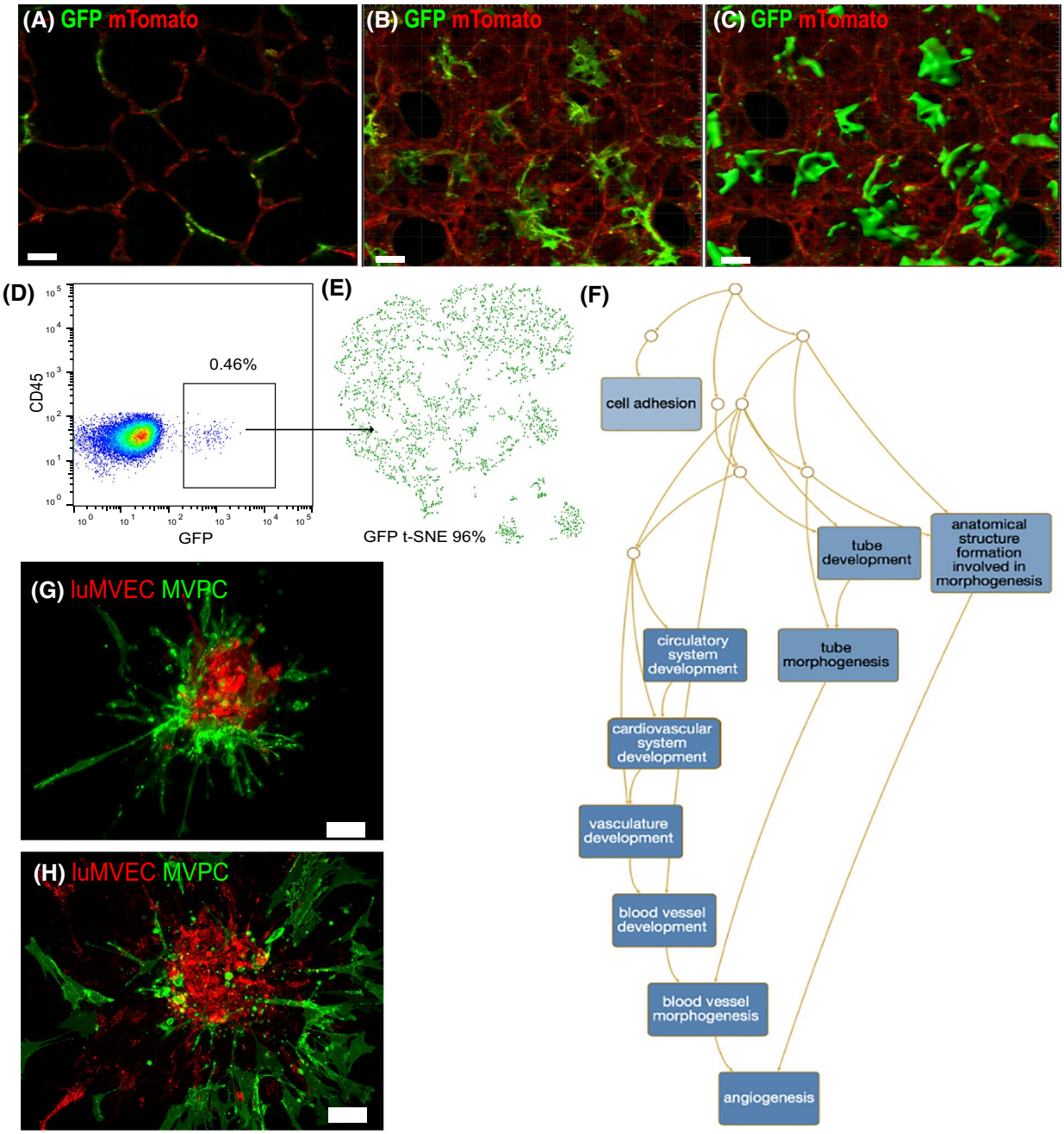

FIGURE 1 Isolated Abcg2^{pos} MVPC have angiogenic transcriptional signatures and potential. A-C, *Abcg2-Cre-ERT2 Rosa26mTmG* WT mice were induced with intraperitoneal tamoxifen. Two days post induction mice were sacrificed, and lungs agarose inflated using constant pressure, to obtain lung tissue for precision cut lung slices for two-photon imaging. Membrane labeled eGFP MVPC were visible in green and mTomato lung tissue was detected in the red channel. A, Representative 2 μM section through the lung tissue Z stack. B and C, Reconstruction of the three-dimensional lung image naïve and with a Gaussian filter. Scale and grid dimension = 20 μM. D, *Abcg2-Cre-ERT2 Rosa26mTmG* WT mice were induced with intraperitoneal tamoxifen. Two days post induction mice were sacrificed, and lung tissue digested to a single cell suspension for cell sorting to obtain the eGFP labeled cells. E, t-SNE plot depicting CD45^{neg} eGFP labeled cells analyzed using 10x single cell RNA sequencing. F, GO clustering analysis. G and H, Angiogenic sprouting and migration potential of MVPC was defined by co-culture three-dimensional spheroid assays

MOVIE). To further define the nature of the Abcg2 MVPC, single cell RNA sequencing was performed. A single cell suspension of murine lung tissue was sorted to separate eGFP expressing cells (Figure 1D). Transcriptomes of 4017 $CD45^{neg}$ eGFP cells were sequenced to a mean of 315 576 reads/cell (a median of 953 genes per cell) using the 10xGenomics platform. Using the 10xGenomics Loupe Cell Browser, we determined that 96% of $CD45^{neg}$ eGFP cells expressed a transcriptome indicative of multipotent mesenchymal vascular progenitors (Figure 1E,F and Table 1). Key determinants included *Ly6a* (ScaI), *Flk1, Flt1 Cdh5, Tek* (Tie2), *Eng* (CD105), *Pecam* (CD31), *Foxf1, Lyve1, Itga1, Edn1, S1pr1, and BMPR2* (Table 1; Supporting Figure S1).[41-45] Additionally, this population lacked significant expression of *Car4*,[46] *Dll4*,[47-49] demonstrated expression of *c-Kit* and the angiogenic molecule *CD93*[50] (Supporting Figure S1). Hierarchical clustering and GO analysis was performed and identified categories associated with angiogenic processes (Figure 1F and Supporting Table S2) including: regulation of endothelial barrier, endothelial cell development (including lymphatic), lung vasculature development/morphogenesis, vasculogenesis, sprouting angiogenesis and positive regulation of cell or endothelial cell migration, regulation of BMP signaling pathway, response to hypoxia, and mesenchyme development. Categories associated with epithelial regulation were: lung alveolus development, branching morphogenesis of an epithelial tube and positive/negative regulation of epithelial cell differentiation and migration (Supporting Table S2). In vitro three-dimensional vascular spheroid co-culture analysis demonstrated the tube forming and migratory potential of murine MVPC relative to lung MVEC (Figure 1G,H). Thus, MVPC play a regulatory role in the lung microvascular niche, comprise a multipotent vascular progenitor phenotype as well as directly participate in adaptive angiogenesis.

To define a functional significance for the lung MVPC population, we selectively depleted these cells in vivo by engineering mice, in which *Abcg2-Cre-ERT2* was crossed to $^{fl}stop^{fl}$ *DTA* and a reporter *Rosa26mTmG*.[20,51] Mice were administered a single dose of tamoxifen (0.02 mg/g) and lung tissue sections were then analyzed for changes in tissue architecture.

TABLE 1 Top 50 genes in GFPpos cells

Gene	Log2 Fold Change	*P*-value	Gene	Log2 Fold Change	*P*-value
Scgb1a1	−7.223871011	1.44E-107	*Itga1*	5.409905416	6.08E-25
Ptprb	6.421083773	9.79E-33	*Fmo1*	5.418503357	6.22E-25
Calcrl	6.311036351	1.34E-31	*Scn7a*	5.622690678	8.43E-25
Tmem100	6.196069716	7.24E-31	*Icam2*	5.434842991	1.38E-24
Cdh5	6.114112411	5.51E-30	*Sema3c*	5.404884676	2.12E-24
Cxcl12	6.098934754	2.82E-29	*Egfl7*	5.061042323	2.97E-24
Tspan7	6.1222942	3.30E-29	*Thbd*	5.145866085	8.66E-24
Clec14a	6.128228101	3.30E-29	*Ace*	5.064925166	8.83E-24
Cldn5	5.793411224	7.32E-29	*Adgrf5*	4.904596787	3.27E-23
Plvap	6.032582526	8.18E-29	*Cd93*	4.950572449	6.13E-23
Ramp2	5.834408603	1.01E-28	*Slco2a1*	5.021742097	7.85E-23
Aqp1	5.911595357	1.29E-28	*Esam*	5.107124152	7.95E-23
Tie2/Tek	6.244118402	2.09E-28	*Sca1/Ly6a*	4.759290772	3.16E-22
Eng	5.962395401	2.35E-28	*Bmpr2*	4.778387384	4.01E-22
Lyve1	6.433252167	6.94E-28	*Edn1*	5.021552994	5.60E-22
Foxf1	6.024244291	5.74E-27	*Acvrl1*	4.73362789	6.45E-22
Pecam1	5.630994125	5.82E-27	*Sparcl1*	4.897329011	1.11E-21
Gpihbp1	5.803532867	7.70E-27	*Ctla2a*	4.736117235	1.22E-21
Tm4sf1	5.55159617	1.19E-26	*S1pr1*	4.708281041	4.84E-21
Ly6c1	5.646064165	1.23E-26	*Cavin1*	4.737835792	5.87E-21
Cyyr1	5.603486745	4.69E-26	*Id3*	4.619945449	7.65E-21
Efnb2	5.775305044	5.70E-26	*Id1*	4.723059956	9.32E-21
Hmcn1	5.763531721	9.67E-26	*Vwf*	4.949834686	1.02E-20
Hpgd	5.40633778	1.26E-25	*Flt1*	4.574584046	1.08E-20
Cav1	5.319645308	3.29E-25	*Pltp*	4.510079688	1.51E-20

Distal alveolar simplification was evident 1 month following MVPC depletion and demonstrated by the presence of increased mean linear intercept (MLI) and decreased fractional lung volume in the absence of detectable pulmonary hypertension as assessed by Fulton Index (Figure 2A-D; Supporting Figure S2A). About 15 months following MVPC depletion loss of distal lung structure was exacerbated and resembled an emphysematous-like phenotype (Figure 2E,F). The increased mean linear intercept was associated with increased compliance and decreased resistance (Figure 2G-I). Thus, targeted depletion of Abcg2 lineage labeled MVPC negatively impacted distal lung structure, suggesting they are required for the maintenance of distal lung parenchymal structure.

To address the role of Abcg2 MVPC in the maintenance of distal lung structure, we exposed WT and MVPC depleted mice to one month of cigarette smoke (CSE). Neither WT nor DTA mice demonstrated an increase in MLI or mean surface to volume ratio (Figure 2J,K) relative to the room air (RA) baseline. However, WT mice responded to CSE with adaptive vascular remodeling characterized by increased microvessel density and muscularization, which was not detected in the DTA mice (Figure 2L-N; 0-50 μM; Supporting Figure S2G-I). These data highlight two pivotal findings, that adaptive microvascular remodeling preceded loss of distal lung tissue structure and that MVPC are required for adaptive angiogenesis in response to injury.

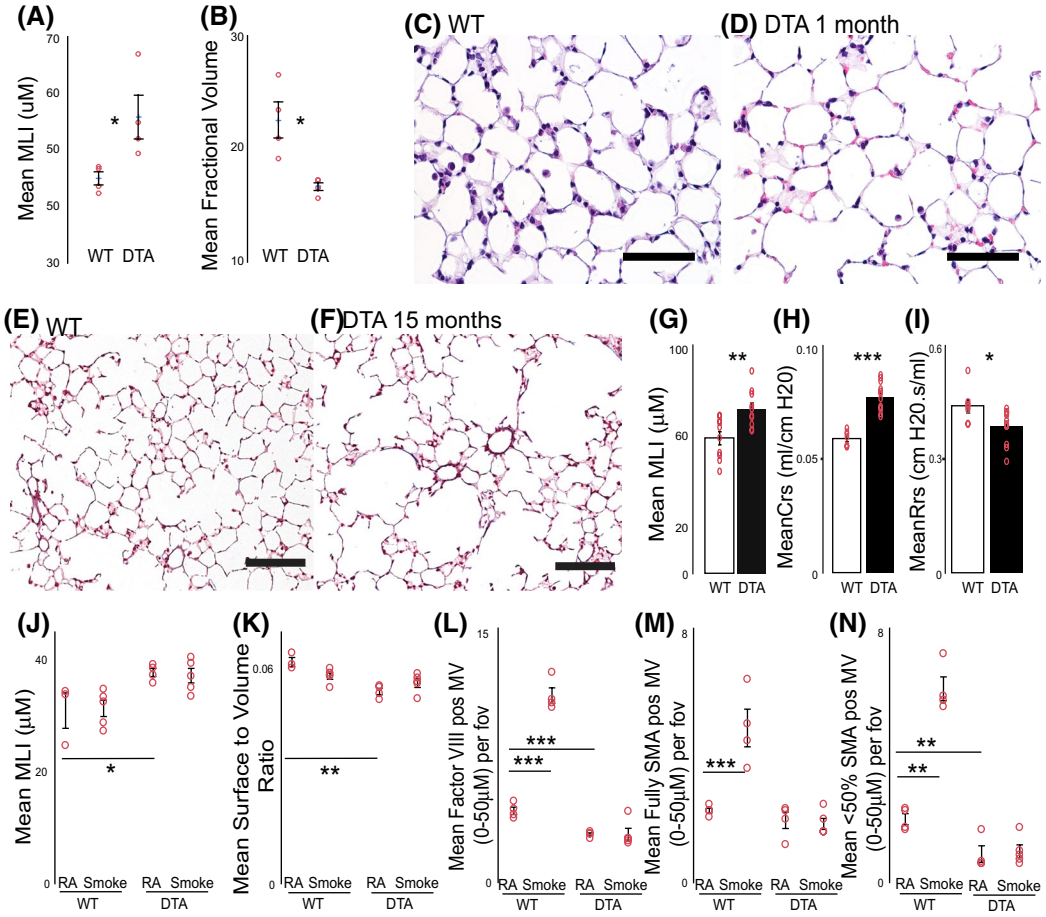

FIGURE 2 Targeted depletion of MVPC effect on distal lung structure and adaptive angiogenesis. WT or $^{f/f}$STOP DTA *Abcg2-Cre-ERT2 Rosa26mTmG* mice were induced with intraperitoneal tamoxifen. One month or 15 months following induction mice were sacrificed, and lungs agarose inflated using constant pressure, to obtain lung tissue for histological and immunofluorescent analyses. n = 4,5 (1 month). A, Quantitation of MLI. B, Fractional volume, the fraction of an image that is occupied by lung tissue. C and D, Representative H&E stained lung tissue sections. Scale bar = 50 μM. n = 10, 12 (15 months) E and F, Representative H&E stained lung tissue sections. Scale bar = 100 μM. G. Quantitation of MLI. H and I, Mean compliance and resistance measured by FlexiVent. WT, $^{f/f}$STOP DTA mice were induced with intraperitoneal tamoxifen, 2 weeks later mice were exposed to cigarette smoke for four weeks. Six weeks following induction mice were sacrificed, and lungs agarose inflated using constant pressure, to obtain lung tissue for histological analyses. n = 4, 9, 4, 5. K, Quantitation of MLI and L, surface to volume ratio. Immunostaining was performed on lung tissue sections to detect smooth muscle alpha actin (SMA) and F8 positive microvessels as well as muscularization. M-O, The immune-positive microvessels were counted per field of view. A 6-8 sections of 20 field of view (f.o.v.) per section were evaluated

3.2 | Activation of Wnt signaling in MVPC is sufficient to cause emphysema-like distal lung remodeling and exacerbate vascular Injury

Chronic lung diseases, including emphysema, are associated with abnormal regulation of developmental signaling cascades, including Wnt/β-catenin.[52-54] We previously demonstrated that activation of canonical Wnt signaling in murine MVPC promoted microvascular dysfunction.[14] Therefore, to assess whether activation of Wnt/β-catenin signaling in MVPC would exacerbate the emphysematous loss of tissue structure, we employed an endovascular injury model in mice using the vascular endothelial growth factor (VEGF) receptor tyrosine kinase inhibitor, SU5416 (Sugen) in combination with hypoxia exposure.[55-57] VEGF, a proangiogenic and survival factor for endothelial and mesenchymal cells,[58-60] is decreased in COPD in spite of hypoxemia.[61] While Sugen hypoxia could affect multiple cell types, similar to the elastase and other models of emphysema,[62,63] the predominant effect is on the vasculature, specifically lung endothelium.[64]Thus, inhibition of VEGF receptor signaling in combination with hypoxia exposure is complex and results in significant endothelial injury, apoptosis, apoptosis resistant cells[56,64-67] and is a significant contributor to the development of COPD/emphysema and pulmonary hypertension (PH).[68] Additionally, this vascular injury model, differs from smoke in that there is not an initiating inflammatory cascade, the phenotype is a result of a direct vascular injury. Thus, the model was well suited to examine how MVPC modulate the microvascular niche to maintain lung structure and function.

Wnt signaling was activated in MVPC by crossing the Abcg2-Cre-ERT2 driver strain with a floxed Δexon 3 allele of β-catenin, thereby expressing an inducible β-catenin lacking degradation domains.[14,21] The lungs of stabilized β-catenin (βOE) lineage labeled mice were compared to wild-type (WT). Lungs were harvested from a standard three-week model of Sugen with hypoxia exposure and compared to room air (RA) vehicle, RA + Sugen or hypoxia vehicle groups in age matched mice. We found that in response to hypoxia WT mice exhibited predicted responses with increased RVSP, muscularization, and microvessel density (Figure 3A-C). WT mice responded to Sugen + hypoxia, with increased RVSP and characteristic decreased muscularization and microvessel density (Figure 3A-C). Wnt activation in the MVPC significantly increased RVSP in response to Sugen following both RA and hypoxia exposure, while the muscularization and microvessel density were not significantly changed from baseline (Figure 3A-C). In fact, βOE mice exhibited decreased muscularization and microvessel density overall, closely resembling the loss of microvessels by WT mice exposed to Sugen + hypoxia (Figure 3B,C; Supporting Figure S3 and S4). Overall, in contrast to WT, Wnt activation in MVPC blunted the adaptive responses to hypoxia including RVSP and microvessel density. Interestingly, the baseline number of collagen positive microvessels was greater in the βOE lungs vs WT (Figure 3D, Supporting Figure S3D-I). Finally, in the lungs of βOE mice exposed to hypoxia + Sugen, significant findings included decreased microvessel density with increased total collagen content (Figure 3E), areas of subpleural fibrosis (Figure 3F) and MLI (Figure 3G-K). Interestingly, comparing isolated WT to βOE MVPC in a spheroid sprouting angiogenesis assay, the βOE MVPC demonstrated increased tube forming and migratory capacity relative to the WT MVPC (Figure 3L-N). Thus, the microvascular phenotype resulting from abnormal Wnt activation in MVPC coupled to endovascular injury was associated with the appearance of an emphysematous—like phenotype and enhanced perivascular and interstitial fibrosis, thus, exacerbation of injury. These data illustrate the importance of regulated Wnt signaling by MVPC in the maintenance of pulmonary microvascular and alveolar architecture.

3.3 | MVPC directly participate in adaptive microvascular remodeling

Given the marked effect of MVPC on endothelial and vascular function that indicates significant intercellular or paracrine crosstalk, and the difference in sprouting capacity of βOE MVPC, we next performed lineage analysis to evaluate the spatial fate of MVPC in response to vascular injury and remodeling. In both WT and βOE mouse strains, there was evidence of intravascular localization of MVPC following Sugen + hypoxia exposure (Figure 4A,L), as well as close proximity of MVPC with microvessels, especially in regions of bridging and sprouting angiogenesis (Figure 4B,C). In Sugen + hypoxia injured lung tissue eGFP labeled the βOE MVPC lineage derived cells that formed SMA^{neg} structures, resembling microvessels in the distal lung (Figure 4D-I). Many of these structures contained DAPI positive nuclei in their lumen (*), suggesting continuity with the pulmonary circulation. Only the βOE Sugen + hypoxia group developed focal areas of interstitial fibrosis (Figure 4E-G). Further analysis of the structures was performed to identify endothelial investment. Factor VIII or podoplanin was used to distinguish capillary vs lymphatic structures. Factor VIII colocalization with eGFP demonstrated that while some MVPC are present adjacent to capillary microvessels, $eGFP^{POS}$ vascular like structures did not exhibit a capillary endothelial-lined lumen (Figure 4G-I). Podoplanin is expressed by both lymphatic endothelium and alveolar Type 1 cells, however, it is typically used to discern lymphatic from capillary endothelium in the mouse. Podoplanin and eGFP co-localization demonstrated that MVPC did not co-express podoplanin and

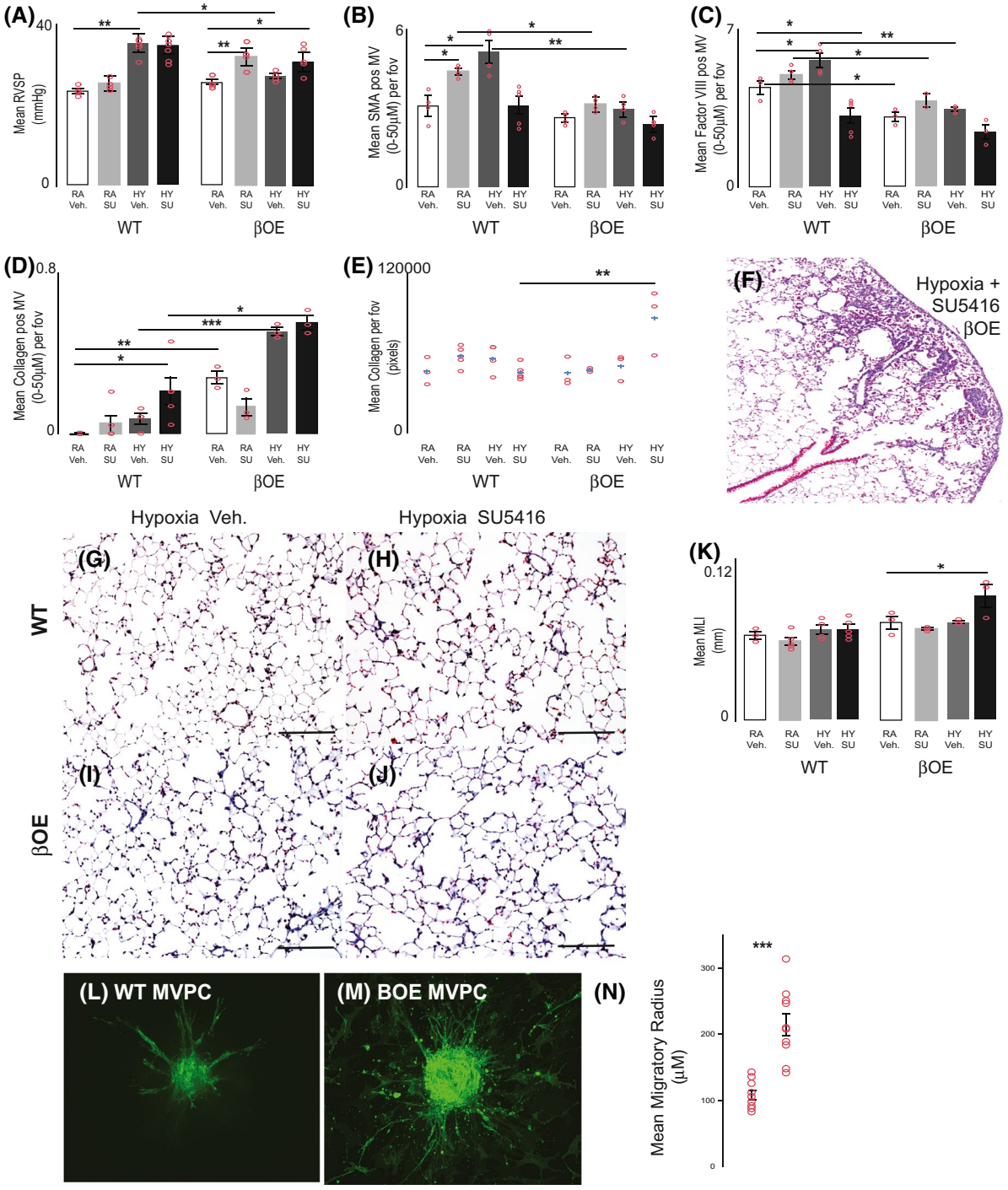

FIGURE 3 Canonical Wnt activation in Abcg2^{pos} MVPC blunted adaptive responses to hypoxia and exacerbated injury following Sugen-hypoxia exposure. Adult WT or βcatenin over expresser (βOE) mice were treated with intraperitoneal tamoxifen. Two weeks following induction mice were grouped for exposure to room air (RA) + CMC vehicle (Veh.), room air + Sugen5416 (SU5416), hypoxia + CMC vehicle (10% oxygen; HY Veh.) or hypoxia + SU5416 (HY SU). Histological and physiological parameters were analyzed after three weeks. A, A pressure transducer was placed in the jugular to the right heart to measure RVSP. Lungs were agarose inflated using constant pressure to obtain lung tissue for histological and immunofluorescent analyses. Immunostaining was performed on lung tissue sections to detect (B) smooth muscle alpha actin (SMA) and (C) F8 positive microvessels as well as muscularization. The immune-positive microvessels were counted per field of view. A 6-8 sections of 20 field of view (f.o.v.) per section were evaluated. D, Trichrome staining was performed on tissue sections and collagen positive microvessels were enumerated. A 6-8 sections of 20 f.o.v. per section were examined. E, Total collagen per f.o.v. was also calculated using FIJI software. F, Representative image of fibrosis in a trichrome stained βOE hypoxia + SU5416 lung section. G-J, Representative trichrome images illustrate distal lung tissue structure. Scale bars = 100 μM. K, MLI was calculated to evaluate simplification of distal lung tissue structure. Data presented as the mean (±SEM). n = 6-9 mice/group. RA Vehicle (white box); RA SU5416 (light grey box); HY Vehicle (dark grey box); HY SU5416 (black box).L-N, Angiogenic sprouting and migration potential of primary eGFP^{pos} MVPC was defined by co-culture three-dimensional spheroid assays (n = 10, 10)

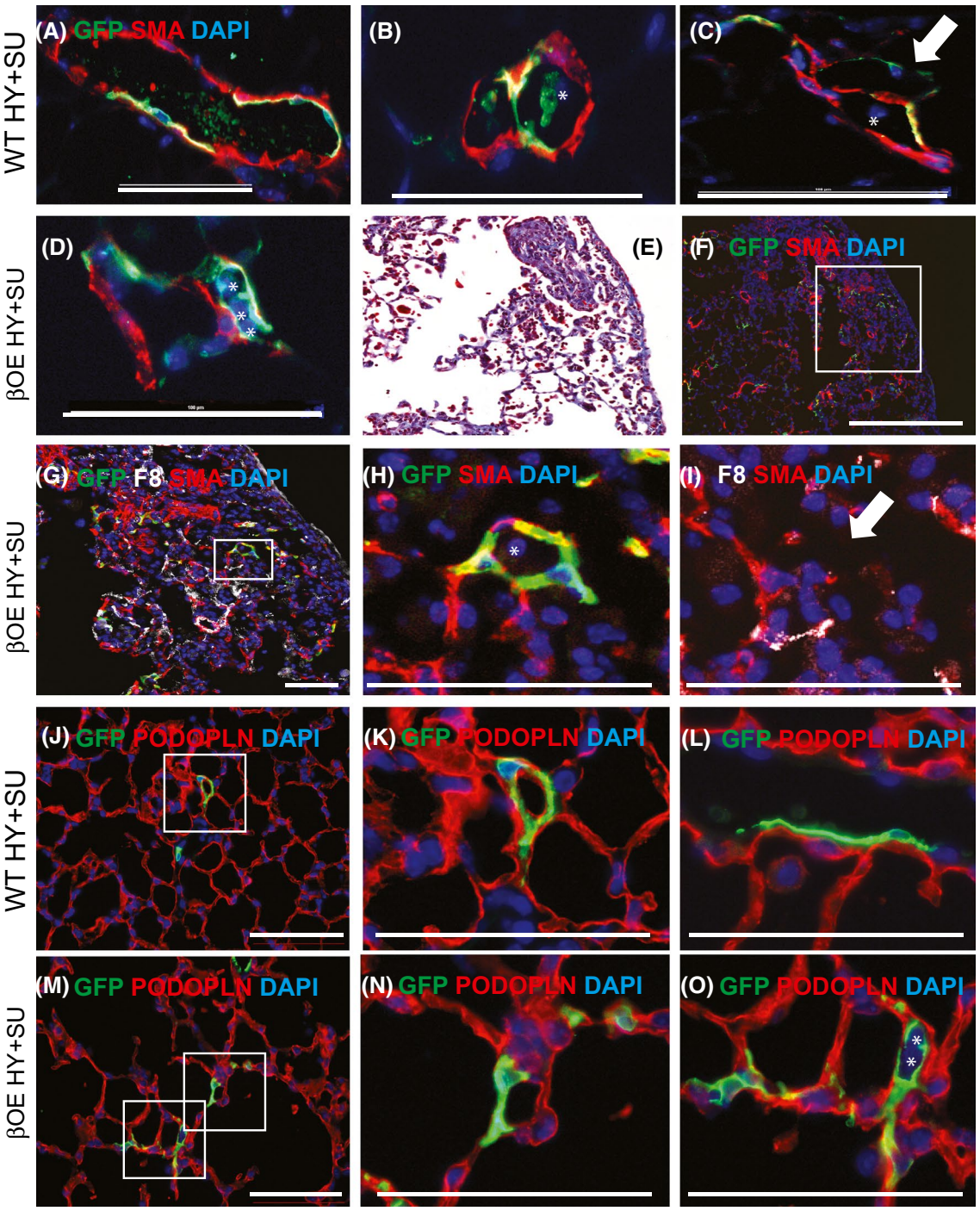

FIGURE 4 MVPC directly participate in de novo angiogenesis following lung injury. Immunostaining was performed on lung tissue sections from room air (RA) + CMC vehicle (Veh.), room air + Sugen5416 (SU5416), hypoxia (10% oxygen) or hypoxia + SU groups to detect eGFP labeled MVPC and lineage derivatives. Costaining was performed to detect SMA positive muscularized vessels, Factor VIII (F8; G&I) or podoplanin (podopln; J-O) positive microvascular endothelium. Representative images from WT or βOE hypoxia + SU groups were presented. A, MVPC migrate along vascular wall. B-D, MVPC form vascular structures via bridging or sprouting adjacent to SMA^{pos} microvessels. E-I, Fibrosis was identified in the βOE hypoxia + SU groups. E, Trichrome staining. F, Immunofluorescent detection of eGFP and SMA. G, Enlarged from F, Immunofluorescent detection of eGFP, SMA, and FactorVIII. H, Enlarged eGFP expressing vascular structure from G. I. Enlarged eGFP F8 negative vascular structure from G, H. J, Immunofluorescent detection of eGFP and podoplanin in WT lungs. K, Enlarged eGFP expressing structures adjacent to podoplanin positive endothelium from J. L, Migrating MVPC do not express podoplanin. M, Immunofluorescent detection of eGFP and podoplanin in βOE lungs enlarged in N and O. N, eGFP adjacent to podoplanin positive endothelium. O, eGFP positive structures lacking podoplanin expressing endothelium. Nuclei are stained with DAPI (blue). The presence of nuclei in MVPC derived structures was indicated by the presence of *. n = 6-9 mice/group. Scale bars = 100 μM

that subgroups of both WT and βOE MVPC derived vascular structures had a lymphatic endothelial lined lumen (Figure 4J-O). Uninjured and control groups were presented in Supporting Figures S4 and S5. MVPC contributed to the genesis of vascular-like structures, however, lacking expression of capillary and lymphatic endothelium.

3.4 | Deregulated expression of an angiogenic profile by COPD MVPC

Following the observation that the lung MVPC played a crucial function in the maintenance of the alveolar architecture, we hypothesized that the gene expression profile of MVPC from COPD patients would exhibit alterations to their angiostasis repertoire. Human MVPC were isolated from explanted lung tissue via ABCG2 enrichment and characterized as previously described, expressing mesenchymal cell surface determinants, lacking hematopoietic, and endothelial determinants as well as forming colonies (CFU-F) (Supporting Tables S3-S5, Supplemental Figure S6E-F).[14,18,69] Global gene expression profiling with hierarchical clustering and GO analysis was performed (Figure 2A; Supporting Figure S6A-D, Supporting Table S5). GO categories associated with angiogenic processes and increased gene expression included: circulatory/cardiovascular system development, vasculature development/morphogenesis, angiogenesis, and positive regulation of cell or endothelial cell proliferation. GO categories associated with angiogenic processes that showed decreased gene expression included: negative regulation of cell proliferation and circulatory/cardiovascular system development. Categories associated with epithelial remodeling that showed increased gene expression were: regulation of epithelial cell migration and proliferation.

Targeted analysis of gene expression by PCR defined distinct changes in Wnt signaling, *AXIN2, PROX1, SFRP1, DKK1, LRP6* by COPD MVPC, as well as the noncanonical ligand *WNT5A,* relative to healthy, indicating that Wnt/β-catenin signaling is upregulated in MVPC (Figure 5B). These findings are in contrast to endothelial and epithelial cells from COPD patients, in which Wnt signaling is decreased.[52,70,71] The Wnt modulators *WLS* and *CREB5* were also decreased in COPD MVPC. Genes associated with modulation of the actin cytoskeleton and migration were also changed between groups. *SVIL* decreased while *EDNRA* and *HMMR* increased (supervillain, endothelin receptor, hyaluronan mediated motility receptor/CD168) in COPD MVPC (Figure 5C). The ligand, *SLIT2*, which influences angiogenesis and directional migration also increased in COPD MVPC, while it's receptor, *ROBO1,* was unchanged.[72,73] Most notably, expression of angiopoietin 1 (*ANGPT1)* was decreased in COPD MVPC suggesting that microvessel stability was impaired. Western blot analysis of normal and COPD MVPC lysates further confirmed higher levels of protein expression of DKK1, WNT5A, and SLIT2 compared to healthy MVPC (Figure 5D). Differentially regulated and interacting signaling pathways were identified using STRING analysis and included canonical Wnt, Robo-Slit, angiopoietins1/2-Tie2/TEK, FGF, TGFβ, BMP, and NOTCH (Figure 5B,C; Supporting Figure S6G; Supporting Table S5). Further analysis demonstrated that Wnt activated murine MVPC recapitulated the human COPD MVPC differential expression of *Dkk1, Prox1, Angpt1*, *Slit2* as well as *Wnt5a* (Figure 5F relative to B). Murine Wnt activated MVPC also expressed significantly increased levels of *Angpt2,* further suggesting microvessel stability was impaired. A comparative summary of gene expression was presented in Figure 5G. Together these results suggest that under the control of Wnt signaling, MVPC regulate cell fate, proliferation, migration, and angiogenesis.

We next tested the direct effects of COPD MVPC on MVEC migration and barrier function in a model of wound injury and repair using an electrical cell-substrate impedance sensing (ECIS) system. The ability of cells to migrate into the denuded area and close the monolayer, as measured by increased resistance, is an indication of structural and functional activity of MVEC. Loss of barrier function and migration are necessary for angiogenesis and repair, whereas the formation of tight junctions and barrier integrity indicate vessel stability.[6,74-77] MVPC were co-cultured with a confluent monolayer of MVEC, which was disrupted using an electrical "wounding" injury (Figure 5E). The rate at which the MVEC barrier formation was recovered following injury was indicated by the slope of change in transcellular resistance relative to that at the time of injury. The rate of MVEC barrier function recovery was decreased by addition of COPD MVPC following injury, compared to addition of healthy MVPC or MVEC alone (Figure 5E). These data support the hypothesis that COPD MVPC decreased MVEC barrier function and may negatively modulate microvascular stability.

The lung vasculature has evolved highly responsive mechanisms to maintain tissue perfusion and oxygen homeostasis. Our data suggest that in response to lung and vascular injury, Wnt signaling in the novel Abcg2^{HI} subset of MVPC regulate adaptive responses of the microvasculature including: angiogenesis vs microvessel rarefaction, muscularization of microvessels or collagen deposition and the MVPC direct contribution to the formation of angiogenic tubes (Figure 6). Therefore, it is reasonable to speculate that the Wnt signaling status and subsequent function of MVPC is regulated by the disease microenvironment, to influence the microvasculature program of adaptation resulting in either repair or remodeling long term.

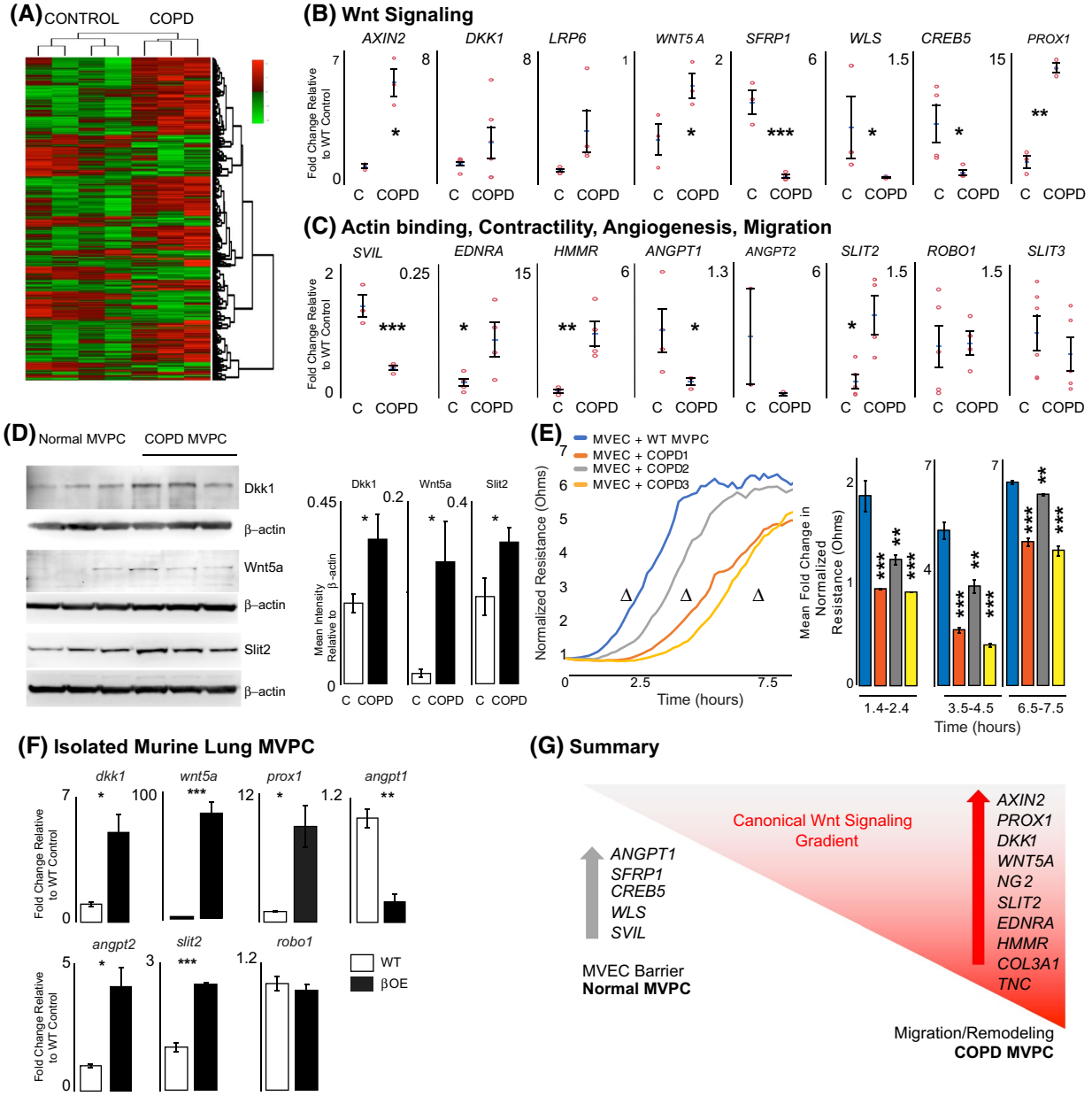

FIGURE 5 Disrupted Wnt signaling in ABCG2^{pos} COPD MVPC disrupts MVEC function. A, Heatmap for differentially expressed genes in MVPC from COPD vs non-diseased lungs (color scale shown at the top right) B and C, Validation of representative genes expressed in COPD ABCG2^{pos} lung MVPC, compared to control, enriched in GO categories of B, Wnt signaling and C, actin binding, contractility, and migration. The mean of combined patient samples per group as well as results for individual samples are presented. n = 3-6 patient samples per group. D, Western blot analysis of Dkk1, Wnt5a and Slit2 protein expression. n = 3, 3. Data presented as the mean ± standard error of mean (SEM). E, Cocultures of pulmonary MVEC and MVPC were analyzed for the effect of control or COPD MVPC on barrier function following injury. MVPC were plated on a monolayer of MVEC at a ratio of 3:1. The groups underwent no injury or an electrical wounding injury using the ECIS system. The presence of COPD MVPC following injury decreased the rate at which barrier formation is recovered. Quantitation of normalized resistance at indicated time points (Δ) was presented in bar graph format. Data presented as mean (±SEM). Controls included MVEC alone and uninjured MVEC. n = 4. F, Murine WT and Wnt activated βOE MVPC were analyzed by PCR to examine the expression of angiogenic transcripts identified as different between control and COPD samples. n = 3, 3. All amplification was normalized to a housekeeping gene and the results presented as mean fold change over control. Data presented as mean ± SEM. G. Representative summary of murine and human PCR data

4 | DISCUSSION

Adult tissue resident vascular precursors are an elusive but important population that have been difficult to isolate and characterize in vivo due to lack of specific markers. Our studies show that Abcg2^{pos} lung mouse adult tissue resident vascular precursors (MVPC) have a defining transcriptome, which may be useful in future studies. To study MVPC

functions, we genetically depleted and lineage traced this population demonstrating that, in vivo, MVPC are necessary for adaptive microvascular remodeling following exposure to cigarette smoke as well as endovascular injury and, when MVPCs are depleted, aged mice demonstrate severe emphysema.

Results from our single cell analyses as well as three-dimensional spheroid assays further defined the Abcg2 lineage labeled population as a multipotent adult vascular progenitor reservoir with rigorous angiogenic potential, relative to lung microvascular endothelial cells (MVEC). While MPC in the developing and adult lung are typically described as influencing epithelial cell processes during morphogenesis or as a potential origin of the myofibroblast lineage during adult tissue remodeling, our previous studies highlighted a role of ABCG2^{pos} MVPC in the maintenance and regulation of microvascular homeostasis.[14] The existence of these vascular progenitors was initially demonstrated by our group and others via the identification of a lung "side population" by flow cytometry, and definition that the membrane expression of Abcg2 transporter conferred this phenotype.[18,36-39] Further identification of differentiated and progenitor mesenchymal subpopulations, and understanding of their importance in tissue remodeling has more recently been aided by single cell transcriptome analysis in adult murine models of fibrotic injury.[78]

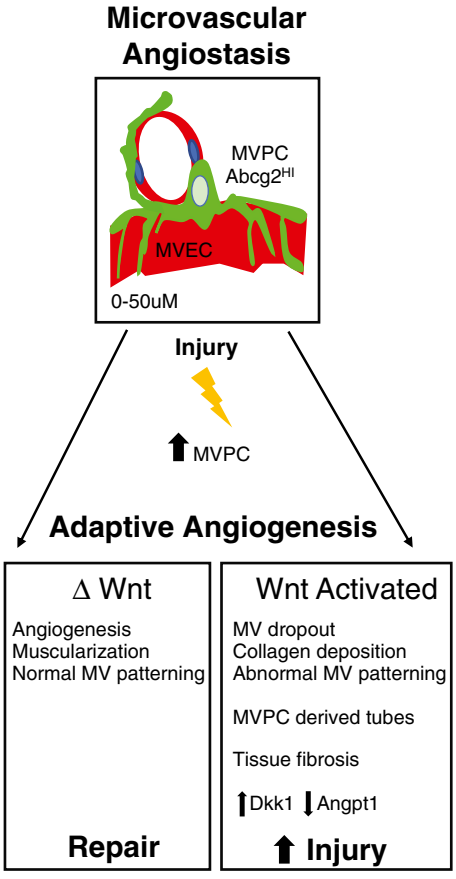

FIGURE 6 Wnt signaling in the Abcg2^{HI} MVPC regulate adaptive responses of the microvasculature. Wnt signaling and function of MVPC is regulated by the disease microenvironment, to influence the microvascular program of adaptation resulting in either repair or remodeling. The microvascular program of adaptation includes: angiogenesis vs microvessel rarefaction, muscularization of microvessels or collagen deposition and the MVPC direct contribution to the formation of angiogenic tubes. MVPC depicted in green and microvascular endothelial cells (MVEC) in red

The function of adaptive angiogenesis is the "structural adaptation" or "angioadaptation" of the vascular network to provide adequate oxygenation to tissues in response to injury or stress.[8] The processes of angiogenesis, vascular remodeling or regression and pruning are necessary in normal angiostasis, tissue repair/regeneration, and the pathogenesis of disease processes. The genetic depletion of MVPC decreased adaptive microvascular endothelial angiogenesis in response to cigarette smoke exposure,[79] while Wnt activation in these cells blunted the typical pro-angiogenic response to physiologic hypoxia in vivo. Stabilized expression of Wnt/β-catenin in MVPC converted the cells to a proangiogenic phenotype both in vitro and in vivo, a property that exacerbated systemic endovascular injury in mice.

The appearance of mesenchymal derived angiogenic tubular structures driven by this Wnt-dependent phenomenon and endovascular injury correlated with an exacerbated emphysema-like phenotype, characterized by decreased microvessel density, increased MLI and interstitial fibrosis. Previously, we reported that Wnt activation in MVPC and the genesis of the derived vascular structures were associated with exacerbated fibrosis and injury in the bleomycin mouse model.[14] In these studies, the presence of Wnt activated MVPC lineage-derived tubes, lacking discernable endothelium, was indicative of their direct contribution to adaptive angiogenesis. The absence of these MVPC derived structures in wild-type mice suggested a defect in vascular patterning. Although their significance is currently unclear, we speculate that the MVPC form transient structures that normally would become endothelialized to resolve injury, while in the presence of activated Wnt signaling they form stabilized structures and contribute to the development of disease. The first concept is supported by studies in bone marrow MSC in the context of wound healing where primitive vascular tubes are thought to prime the network toward the formation of new capillaries.[80,81] The second is supported by the role β-catenin plays in adherens junctions independent of Wnt signaling.[82] Alternatively, these incomplete vascular structures resemble tumor microcirculation and may contribute to vascular dysfunction in chronic lung diseases as they may exhibit varying levels of barrier effectiveness, which in turn influences local inflammation and remodeling.[83] Longer term studies are necessary to understand the significance and function of these MVPC-derived structures.

The combination of tissue simplification and fibrosis observed in our models may also be linked to a net loss of microvessel density, similar to the pathology described for pulmonary vascular disease associated with connective tissue diseases such as systemic sclerosis or combined pulmonary emphysema and fibrosis (CPEF)[84,85] or tubulointerstitial fibrosis.[86] The severity of tissue remodeling in these instances is thought to be influenced by the presence of microvascular dysfunction or vasculopathy.[84,85] Fibrotic remodeling and chronic rejection may also be preceded by loss of microvascular integrity and density following lung transplantation.[87] In COPD, microvascular dysfunction and loss occur not only in the lung, but also systemically, and is invoked in muscle mass wasting and cachexia, which are clinical indicators of increased mortality.[88,89]

Chronic lung diseases, including COPD/emphysema, are associated with abnormal regulation of developmental signaling cascades, including Wnt/β-catenin.[52-54,90-97] Isolated human COPD MVPC exhibited active Wnt signaling. Both human COPD MVPC and murine Wnt activated MVPC expressed markers indicative of adaptive angiogenic phenotype including canonical Wnt targets *Dkk1*, *Prox1*, *Wnt5A,* and decreased angiopoietin 1 (*Angpt1*). In the presence of VEGF inhibition, the timing and level of signaling or environmental co-factors produced by MVPC likely balance the response of the microvascular endothelium as well as repair vs remodeling.[98-101] This interaction may explain why in response to hypoxia the wild-type lungs had typical increased microvascular muscularization vs perivascular collagen deposition in the Wnt activated MVPC lungs. The observation that adaptive angiogenesis in our injury models occurred prior to significant changes in distal lung structure, suggesting that deregulated microvascular patterning plays a role during the onset of tissue pathology. The role of Wnt signaling during vascular homeostasis, regression, repair and remodeling is appreciated with regard to the endothelium[98,99] as it promotes sprouting and tip cell specification with the Notch pathway and delta like ligand 4 (*Dll4*).[47,48,102,103] β-catenin expression is regulated by hypoxia inducible factors (HIFs) and also regulates *VEGF-A* and *Dkk1* expression.[104-107] Together Wnt, VEGF and Notch regulate the balance of vascular regeneration and remodeling in response to injury, in cell-specific and dose-dependent manners.[108] Together these studies support a model in which canonical Wnt signaling regulates the ability of Abcg2 MVPCs to act as vascular progenitor and also to function as regulatory cells, maintaining MVEC function and response to injury.

While VEGF signaling was targeted in these studies as a method to induce endovascular injury, specifically defining the vascular cells responsible for the phenotype is likely complicated by effects on both the endothelium and mesenchyme.[60] Additionally, while the exacerbation of remodeling following vascular injury was demonstrated in the Wnt activated MVPC strain, the specific stimuli that initiated the cascades that led to the simplification of the distal lung microvasculature and epithelium have not been defined, highlighting a need for further evaluation. Ongoing studies in our lab are designed to better understand the complexity of MVPC function as well as how changes in MVPC signaling influence the diverse cell populations in the lung including microvascular endothelium, vascular smooth muscle, alveolar epithelium (Type 1 & 2), additional mesenchymal populations (fibroblasts, myofibroblasts, and lipofibroblasts) as well as respective progenitors. Based on these data demonstrating the negative impact of sustained Wnt activation in MVPC on the microvasculature following injury, relative to the therapeutic effect of pan activation of Wnt signaling in rodent models of experimental emphysema,[70] it is plausible that the context of Wnt signaling, influences overall vascular outcomes.

In summary, these results demonstrated the significance of Abcg2^{pos} MVPC in the microvascular niche and the impact of canonical Wnt signaling on the function of MVPC during angiostasis as well as adaptive angiogenesis. Thus, our model is useful to explore the basic mechanisms of the disease onset and progression. Understanding Wnt signaling in MVPC coupled to their regulation of MVEC as well as vascular smooth muscle and epithelium will be important to identify novel targets to facilitate microvascular repair and pulmonary tissue function.

ACKNOWLEDGMENTS

The authors would like to extend thanks to Drs. Pippa Marrack and Darrell Kotton for helpful discussion and Kathleen Gavin for her critical review of the manuscript. The authors would like to extend our greatest appreciation for the advanced microscopy training provided by Jordan Jacobelli, Keegan Walhood (Keyence), single cell informational tutorials to James Scott-Browne and Moumita Ghosh as well as expert technical assistance provided by J. Harral, E. Staker, C. Gaskill, E. Beatman, R. Berman, N. Putz, M. Majka, S. Shay, C. Moore, Catherine E. Alford and the Flow Cytometry Special Resource Center, Department of Pathology and Laboratory Medicine, Veterans Affairs Tennessee Valley Healthcare System, Nashville, TN; K. Helm, C. Childs, L. Acosta, D. Baturin, and the University of Colorado Cancer Center's Flow Cytometry Shared Resource; K. Diener, B. Gao and A. Doan in the University of Colorado Cancer Center's Genomics Core. The podoplanin monoclonal antibody developed by A. G. Farr was obtained from the Developmental Studies Hybridoma Bank, created by the NICHD of the NIH and maintained at the University of Iowa, Department of Biology, Iowa City, IA 52242.

CONFLICT OF INTEREST

The authors have no conflicts of interest to declare.

AUTHOR CONTRIBUTIONS

Conceptualization, S.M. Majka, M.E. Summers; Methodology, M.E. Summers, B.W. Richmond, S. Menon, R.M. Sheridan, S.A. Majka, J.A. Bastarache, J.D. West, S. De Langhe, P. Geraghty, D.J. Klemm, H.W. Chu, R.S. Friedman, Y.K. Tao, R.F. Foronjy, S.M. Majka; Investigation, M.E. Summers, B.W. Richmond, M.M. Taketo, J.A. Kropski, S. Menon, R.M. Sheridan, S.A. Majka, J.A. Bastarache, J. D. West, S. De Langhe, P. Geraghty, D.J. Klemm, H.W. Chu, R.S. Friedman, Y.K. Tao, R.F. Foronjy, S.M. Majka; Writing Original Draft, S.M. Majka, M.E. Summers, D.J. Klemm, R.F. Foronjy; Writing - Review & Editing, S.M. Majka, M.E. Summers, B.W. Richmond, J.A. Kropski, J.A. Bastarache, R.F. Foronjy; Funding Acquisition, S.M. Majka; Resources, J.A. Kropski, B.W. Richmond, M.M. Taketo, Y.K. Tao, R.F. Foronjy; Supervision, S.M. Majka.

REFERENCES

1. Sabit R, Bolton CE, Edwards PH, et al. Arterial stiffness and osteoporosis in chronic obstructive pulmonary disease. *Am J Respir Crit Care Med*. 2007;175:1259-1265.
2. McAllister DA, Maclay JD, Mills NL, et al. Arterial stiffness is independently associated with emphysema severity in patients with chronic obstructive pulmonary disease. *Am J Respir Crit Care Med*. 2007;176:1208-1214.
3. Barr RG, Mesia-Vela S, Austin JHM, et al. Impaired flow-mediated dilation is associated with low pulmonary function and emphysema in ex-smokers: the Emphysema and Cancer Action Project (EMCAP) Study. *Am J Respir Crit Care Med*. 2007;176:1200-1207.
4. Yu N, Wei X, Li Y, Deng L, Jin C-W, Guo Y. Computed tomography quantification of pulmonary vessels in chronic obstructive pulmonary disease as identified by 3D automated approach. *Medicine*. 2016;95:e5095.
5. Alford SK, van Beek EJR, McLennan G, Hoffman EA. Heterogeneity of pulmonary perfusion as a mechanistic image-based phenotype in emphysema susceptible smokers. *Proc Natl Acad Sci U S A*. 2010;107:7485-7490.
6. Carmeliet P, Jain RK. Molecular mechanisms and clinical applications of angiogenesis. *Nature*. 2011;473:298-307.
7. Han H-C. Twisted blood vessels: symptoms, etiology and biomechanical mechanisms. *J Vasc Res*. 2012;49:185-197.
8. Secomb TW, Alberding JP, Hsu R, Dewhirst MW, Pries AR. Angiogenesis: an adaptive dynamic biological patterning problem. *PLoS Comput Biol*. 2013;9:e1002983.
9. Akeson AL, Wetzel B, Thompson FY, et al. Embryonic vasculogenesis by endothelial precursor cells derived from lung mesenchyme. *Dev Dyn*. 2000;217:11-23.
10. Gebb SA, Shannon JM. Tissue interactions mediate early events in pulmonary vasculogenesis. *Dev Dyn*. 2000;217:159-169.
11. Schachtner SK, Wang Y, Scott Baldwin H. Qualitative and quantitative analysis of embryonic pulmonary vessel formation. *Am J Respir Cell Mol Biol*. 2000;22:157-165.
12. Zhang W, Menke DB, Jiang M, et al. Spatial-temporal targeting of lung-specific mesenchyme by a Tbx4enhancer. *BMC Biol*. 2013;11:111.
13. Kumar ME, Bogard PE, Espinoza FH, Menke DB, Kingsley DM, Krasnow MA. Defining a mesenchymal progenitor niche at single cell resolution. *Science*. 2014;346:1258810.
14. Gaskill CF, Carrier EJ, Kropski JA, et al. Disruption of lineage specification in adult pulmonary mesenchymal progenitor cells promotes microvascular dysfunction. *J Clin Investig*. 2017;127:2262-2276.
15. Xie T, Liang J, Liu N, et al. Transcription factor TBX4 regulates myofibroblast accumulation and lung fibrosis. *J Clin Investig*. 2016;126:3063-3079.
16. Kramann R, Schneider RK, DiRocco DP, et al. Perivascular Gli1+ progenitors are key contributors to injury-induced organ fibrosis. *Cell Stem Cell* 16:51-66.
17. El Agha E, Kramann R, Schneider RK, et al. Mesenchymal stem cells in fibrotic disease. *Cell Stem Cell* 21:166-177.
18. Marriott S, Baskir RS, Gaskill C, et al. ABCG2(pos) lung mesenchymal stem cells are a novel pericyte subpopulation that contributes to fibrotic remodeling. *Am J Physiol Cell Physiol*. 2014;307:C684-C698.
19. Gaskill C, Marriott S, Pratap S, et al. Shared gene expression patterns in mesenchymal progenitors derived from lung and epidermis in pulmonary arterial hypertension: identifying key pathways in pulmonary vascular disease. *Pulm Circ*. 2016;6:483-497.
20. Fatima S, Zhou S, Sorrentino BP. Abcg2 expression marks tissue-specific stem cells in multiple organs in a mouse progeny tracking model. *Stem Cells*. 2012;30:210-221.
21. Harada N, Tamai Y, Ishikawa T, et al. Intestinal polyposis in mice with a dominant stable mutation of the beta-catenin gene. *Embo J*. 1999;18:5931-5942.
22. Lee CG, Ma B, Takyar S, et al. Studies of vascular endothelial growth factor in asthma and chronic obstructive pulmonary disease. *Proc Am Thorac Soc*. 2011;8:512-515.
23. Voehringer D, Liang H-E, Locksley RM. Homeostasis and effector function of lymphopenia-induced memory-like T cells in constitutively T cell-depleted mice. *J Immunol*. 2008;180:4742-4753.
24. Chow K, Fessel JP, KaoriIhida S, et al. Dysfunctional resident lung mesenchymal stem cells contribute to pulmonary microvascular remodeling. *Pulm Circ*. 2013;3:31-49.
25. Case D, Irwin D, Ivester C, et al. Mice deficient in galectin-1 exhibit attenuated physiological responses to chronic hypoxia-induced pulmonary hypertension. *Am J Physiol Lung Cell Mol Physiol*. 2007;292:L154-164.
26. Jun D, Garat C, West J, et al. The pathology of bleomycin-induced fibrosis is associated with loss of resident lung mesenchymal stem cells that regulate effector T-cell proliferation. *Stem Cells*. 2011;29:725-735.
27. Yoshida T, Mett I, Bhunia AK, et al. Rtp801, a suppressor of mTOR signaling, is an essential mediator of cigarette smoke nduced pulmonary injury and emphysema. *Nat Med*. 2010;16:767-773.
28. Thurlbeck WM. Measurement of pulmonary emphysema. *Am Rev Respir Dis*. 1967;95:752-764.
29. Tanjore H, Degryse AL, Crossno PF, et al. B-catenin in the alveolar epithelium protects from lung fibrosis after intratracheal bleomycin. *Am J Respir Crit Care Med*. 2013;187:630-639.

30. Polosukhin VV, Degryse AL, Newcomb DC, et al. Intratracheal bleomycin causes airway remodeling and airflow obstruction in mice. *Exp Lung Res*. 2012;38:135-146.
31. Newcomb DC, Boswell MG, Reiss S, et al. IL-17A inhibits airway reactivity induced by respiratory syncytial virus infection during allergic airway inflammation. *Thorax*. 2013;68:717-723.
32. McGrath-Morrow SA, Cho C, Soutiere S, Mitzner W, Tuder R. The effect of neonatal hyperoxia on the lung of p21Waf1/Cip1/Sdi1-deficient mice. *Am J Respir Cell Mol Biol*. 2004;30:635-640.
33. Dikalov S, Itani H, Richmond B, et al. Tobacco smoking induces cardiovascular mitochondrial oxidative stress, promotes endothelial dysfunction, and enhances hypertension. *Am J Physiol Heart Circ Physiol*. 2019;316:H639-H646.
34. Dell'Aringa M, Reinhardt RL, Friedman RS, Jacobelli J. Live imaging of IL-4-expressing T follicular helper cells in explanted lymph nodes. In: Reinhardt RL, ed. *Type 2 Immunity: Methods and Protocols*. New York, NY: Springer; 2018:225-235.
35. Asakura A, Rudnicki MA. Side population cells from diverse adult tissues are capable of in vitro hematopoietic differentiation. *Exp Hematol*. 2002;30:1339-1345.
36. Summer R, Fitzsimmons K, Dwyer D, Murphy J, Fine A. Isolation of an adult mouse lung mesenchymal progenitor cell population. *Am J Respir Cell Mol Biol*. 2007;37:152-159.
37. Martin J, Helm K, Ruegg P, Varella-Garcia M, Burnham E, Majka S. Adult lung side population cells have mesenchymal stem cell potential. *Cytotherapy*. 2008;10:140-151.
38. Tadjali M, Zhou S, Rehg J, Sorrentino BP. Prospective isolation of murine hematopoietic stem cells by expression of an Abcg2/GFP allele. *Stem Cells*. 2006;24:1556-1563.
39. Zhou S, Schuetz JD, Bunting KD, et al. The ABC transporter Bcrp1/ABCG2 is expressed in a wide variety of stem cells and is a molecular determinant of the side-population phenotype. *Nat Med*. 2001;7:1028-1034.
40. Liu W-H, Liu H-B, Gao D-K, et al. ABCG2 protects kidney side population cells from hypoxia/reoxygenation injury through activation of the MEK/ERK pathway. *Cell Transplant*. 2013;22:1859-1868.
41. Kumar A, D'Souza SS, Moskvin OV, et al. Specification and diversification of pericytes and smooth muscle cells from mesenchymoangioblasts. *Cell Rep*. 2017;19:1902-1916.
42. Cossu G, Bianco P. Mesoangioblasts — vascular progenitors for extravascular mesodermal tissues. *Curr Opin Genet Dev*. 2003;13:537-542.
43. Patel J, Seppanen Elke J, Rodero Mathieu P, et al. Functional definition of progenitors versus mature endothelial cells reveals key SoxF-dependent differentiation process. *Circulation*. 2017;135:786-805.
44. Patel J, Donovan P, Khosrotehrani K. Defining tissue resident vascular stem cells. *Oncotarget*. 2017;8:84618-84619.
45. Ng ML, Yarla NS, Menschikowski M, Sukocheva OA. Regulatory role of sphingosine kinase and sphingosine-1-phosphate receptor signaling in progenitor/stem cells. *World J Stem Cells*. 2018;10:119-133.
46. Vila Ellis L, Cain MP, Hutchison V, et al. Epithelial vegfa specifies a distinct endothelial population in the mouse lung. *Dev Cell*. 2020;52:617-630.e6.
47. Corada M, Nyqvist D, Orsenigo F, et al. The Wnt/β-catenin pathway modulates vascular remodeling and specification by upregulating Dll4/notch signaling. *Dev Cell*. 2010;18:938-949.
48. Hellström M, Phng L-K, Hofmann JJ, et al. Dll4 signalling through Notch1 regulates formation of tip cells during angiogenesis. *Nature*. 2007;445:776-780.
49. Travisano SI, Oliveira VL, Prados B, et al. Coronary arterial development is regulated by a Dll4-Jag1-EphrinB2 signaling cascade. *eLife*. 2019;8:e49977.
50. Pill K, Hofmann S, Redl H, Holnthoner W. Vascularization mediated by mesenchymal stem cells from bone marrow and adipose tissue: a comparison. *Cell Regen*. 2015;4:8.
51. Buch T, Heppner FL, Tertilt C, et al. A Cre-inducible diphtheria toxin receptor mediates cell lineage ablation after toxin administration. *Nat Meth*. 2005;2:419-426.
52. Baarsma HA, Skronska-Wasek W, Mutze K, et al. Noncanonical WNT-5A signaling impairs endogenous lung repair in COPD. *J Exp Med*. 2017;214:143-163.
53. Konigshoff M, Eickelberg O. WNT signaling in lung disease. *Am J Respir Cell Mol Biol*. 2010;42:21-31.
54. Yin Y, White AC, Huh S-H, et al. An FGF–WNT gene regulatory network controls lung mesenchyme development. *Dev Biol*. 2008;319:426-436.
55. Fong TAT, Shawver LK, Sun L, et al. SU5416 is a potent and selective inhibitor of the vascular endothelial growth factor receptor (Flk-1/KDR) that inhibits tyrosine kinase catalysis, tumor vascularization, and growth of multiple tumor types. *Can Res*. 1999;59:99.
56. Tuder RM, Zhen L, Cho CY, et al. Oxidative Stress and Apoptosis Interact and Cause Emphysema Due to Vascular Endothelial Growth Factor Receptor Blockade. *Am J Respir Cell Mol Biol*. 2003;29:88-97.
57. Bloodworth N, Clark CR, West JD, et al. Bone marrow–derived proangiogenic cells mediate pulmonary arteriole stiffening via serotonin 2B receptor dependent mechanism. *Circ Res*. 2018;123(12):e51-e64.
58. Kotch LE, Iyer NV, Laughner E, Semenza GL. Defective vascularization of HIF-1α-null embryos is not associated with VEGF deficiency but with mesenchymal cell death. *Dev Biol*. 1999;209:254-267.
59. Ylikorkala A, Rossi DJ, Korsisaari N, et al. Vascular abnormalities and deregulation of VEGF in Lkb1-deficient mice. *Science*. 2001;293:1323-1326.
60. Majka S, Fox K, McGuire B, Crossno J, McGuire P, Izzo A. Pleiotropic role of VEGF-A in regulating fetal pulmonary mesenchymal cell turnover. *Am J Physiol Lung Cell Mol Physiol*. 2006;290:L1183-L1192.
61. Suzuki M, Betsuyaku T, Nagai K, et al. Decreased airway expression of vascular endothelial growth factor in cigarette smoke-induced emphysema in mice and COPD patients. *Inhalation Toxicol*. 2008;20:349-359.
62. Bingle L, Richards RJ, Fox B, Masek L, Guz A, Tetley TD. Susceptibility of lung epithelium to neutrophil elastase: protection by native inhibitors. *Mediators Inflamm*. 1997;6:345-354.
63. Chetty A, Davis P, Infeld M. Effect of elastase on the directional migration of lung fibroblasts within a three-dimensional collagen matrix. *Exp Lung Res*. 1995;21:889-899.
64. Kasahara Y, Tuder RM, Taraseviciene-Stewart L, et al. Inhibition of VEGF receptors causes lung cell apoptosis and emphysema. *J Clin Investig*. 2000;106:1311-1319.
65. Taraseviciene-Stewart L, Kasahara Y, Alger L, et al. Inhibition of the VEGF receptor 2 combined with chronic hypoxia causes

cell death-dependent pulmonary endothelial cell proliferation and severe pulmonary hypertension. *Faseb J*. 2001;15:427-438.
66. Vitali SH, Hansmann G, Rose C, et al. The Sugen 5416/hypoxia mouse model of pulmonary hypertension revisited: long-term follow-up. *Pulm Circ*. 2014;4:619-629.
67. Tang K, Rossiter HB, Wagner PD, Breen EC. Lung-targeted VEGF inactivation leads to an emphysema phenotype in mice. *J Appl Physiol*. 2004;97:1559.
68. Polverino F, Celli BR, Owen CA. COPD as an endothelial disorder: endothelial injury linking lesions in the lungs and other organs? (2017 Grover Conference Series). *Pulm Circ*. 2018;8:2045894018758528.
69. Gaskill C, Majka SM. A high-yield isolation and enrichment strategy for human lung microvascular endothelial cells. *Pulm Circ*. 2017;7:108-116.
70. Kneidinger N, Yildirim AO, Callegari J, et al. Activation of the WNT/β-catenin pathway attenuates experimental emphysema. *Am J Respir Crit Care Med*. 2011;183:723-733.
71. Wang R, Ahmed J, Wang G, et al. Down-regulation of the canonical Wnt B-catenin pathway in the airway epithelium of healthy smokers and smokers with COPD. *PLoS One*. 2011;6:e14793.
72. Chen C-Y, Tsai C-H, Chen C-Y, Wu Y-H, Chen C-P. Human placental multipotent mesenchymal stromal cells modulate placenta angiogenesis through Slit2-Robo signaling. *Cell Adh Migr*. 2016;10:66-76.
73. Rama N, Dubrac A, Mathivet T, et al. Slit2 signaling through Robo1 and Robo2 is required for retinal neovascularization. *Nat Med*. 2015;21:483-491.
74. Adams RH, Alitalo K. Molecular regulation of angiogenesis and lymphangiogenesis. *Nat Rev Mol Cell Biol*. 2007;8:464-478.
75. Armulik A, Abramsson A, Betsholtz C. Endothelial/pericyte interactions. *Circ Res*. 2005;97:512-523.
76. Carmeliet P. Mechanisms of angiogenesis and arteriogenesis. *Nat Med*. 2000;6:389-395.
77. DiPietro LA. Angiogenesis and scar formation in healing wounds. *Curr Opin Rheumatol*. 2013;25:87-91.
78. Xie T, Wang Y, Deng N, et al. Single-cell deconvolution of fibroblast heterogeneity in mouse pulmonary fibrosis. *Cell Rep*. 2018;22:3625-3640.
79. Seimetz M, Parajuli N, Pichl A, et al. Cigarette smoke-induced emphysema and pulmonary hypertension can be prevented by phosphodiesterase 4 and 5 inhibition in mice. *PLoS One*. 2015;10:e0129327.
80. Dufourcq P, Descamps B, Tojais NF, et al. Secreted frizzled-related protein-1 enhances mesenchymal stem cell function in angiogenesis and contributes to neovessel maturation. *Stem Cells*. 2008;26:2991-3001.
81. Mendez JJ, Ghaedi M, Sivarapatna A, et al. Mesenchymal stromal cells form vascular tubes when placed in fibrin sealant and accelerate wound healing in vivo. *Biomaterials*. 2015;40:61-71.
82. Kam Y, Quaranta V. Cadherin-bound β-catenin feeds into the Wnt pathway upon adherens junctions dissociation: evidence for an intersection between β-catenin pools. *PLoS One*. 2009;4:e4580.
83. Nagy JA, Benjamin L, Zeng H, Dvorak AM, Dvorak HF. Vascular permeability, vascular hyperpermeability and angiogenesis. *Angiogenesis*. 2008;11:109-119.
84. Condliffe R, Howard LS. Connective tissue disease-associated pulmonary arterial hypertension. *F1000Prime Rep*. 2015;7:6.
85. Cottin V, Nunes H, Mouthon L, et al. Combined pulmonary fibrosis and emphysema syndrome in connective tissue disease. *Arthritis Rheum*. 2011;63:295-304.
86. Loganathan K, Salem Said E, Winterrowd E, et al. Angiopoietin-1 deficiency increases renal capillary rarefaction and tubulointerstitial fibrosis in mice. *PLoS One*. 2018;13:e0189433.
87. Nicolls MR, Hsu JL, Jiang X. Microvascular injury after lung transplantation. *Curr Opin Organ Transplant*. 2016;21:279-284.
88. Schrimpf C, Teebken OE, Wilhelmi M, Duffield JS. The role of pericyte detachment in vascular rarefaction. *J Vasc Res*. 2014;51:247-258.
89. Mofarrahi M, Sigala I, Vassilokopoulos T, et al. Angiogenesis-related factors in skeletal muscles of COPD patients: roles of angiopoietin-2. *J Appl Physiol*. 2013;114:1309-1318.
90. Baarsma HA, Boczkowski J, Yildirim AO, Konigshoff M. Fibroblast-derived non-canonical WNT ligands contribute to attenuated alveolar epithelial repair in COPD. *Eur Respir J*. 2014;44:1835.
91. Baarsma HA, Spanjer AIR, Haitsma G, et al. Activation of WNT/β-catenin signaling in pulmonary fibroblasts by TGF-β1 is increased in chronic obstructive pulmonary disease. *PLoS One*. 2011;6:e25450.
92. Bellusci S, Furuta Y, Rush MG, Henderson R, Winnier G, Hogan BL. Involvement of Sonic hedgehog (Shh) in mouse embryonic lung growth and morphogenesis. *Development*. 1997;124:53-63.
93. Chilosi M, Poletti V, Rossi A. The pathogenesis of COPD and IPF: Distinct horns of the same devil? *Respir Res*. 2012;13:3.
94. Fernandez IE, Eickelberg O. New cellular and molecular mechanisms of lung injury and fibrosis in idiopathic pulmonary fibrosis. *Lancet*. 2012;380:680–688.
95. Kneidinger N, Yildirim AO, Callegari J, et al. Activation of the WNT/B-catenin pathway attenuates experimental emphysema. *Am J Respir Crit Care Med*. 2011;183:723-733.
96. Pepicelli CV, Lewis PM, McMahon AP. Sonic hedgehog regulates branching morphogenesis in the mammalian lung. *Curr Biol*. 1998;8:1083-1086.
97. Shu W, Jiang YQ, Lu MM, Morrisey EE. Wnt7b regulates mesenchymal proliferation and vascular development in the lung. *Development*. 2002;129:4831-4842.
98. Franco CA, Liebner S, Gerhardt H. Vascular morphogenesis: a Wnt for every vessel? *Curr Opin Genet Dev*. 2009;19:476-483.
99. Li R, Beebe T, Jen N, et al. Shear stress-activated Wnt-angiopoietin-2 signaling recapitulated vascular repair in zebrafish embryos. *Arterioscler Thromb Vasc Biol*. 2014;34:2268-2275.
100. Rao S, Lobov I, Vallance J, et al. Obligatory participation of macrophages in an angiopoietin 2-mediated cell death switch. *Development*. 2008;134:4449-4458.
101. Jeansson M, Gawlik A, Anderson G, et al. Angiopoietin-1 is essential in mouse vasculature during development and in response to injury. *J Clin Investig*. 2011;121:2278-2289.
102. Martowicz A, Trusohamn M, Jensen N, et al. Endothelial β-catenin signaling supports postnatal brain and retinal angiogenesis by promoting sprouting, tip cell formation, and VEGFR (vascular endothelial growth factor receptor) 2 expression. *Arterioscler Thromb Vasc Biol*. 2019;39:2273-2288.
103. Mack JJ, Iruela-Arispe ML. NOTCH regulation of the endothelial cell phenotype. *Curr Opin Hematol*. 2018;25:212-218.

104. Awad KS, West JD, de Jesus Perez V, MacLean M. Novel signaling pathways in pulmonary arterial hypertension (2015 Grover Conference Series). *Pulm Circ*. 2016;6:285-294.
105. Birdsey GM, Shah AV, Dufton N, et al. The endothelial transcription factor ERG promotes vascular stability and growth through Wnt/β-catenin signaling. *Dev Cell*. 2015;32:82-96.
106. Krock BL, Skuli N, Simon MC. Hypoxia-induced angiogenesis: good and evil. *Genes Cancer*. 2011;2:1117-1133.
107. Smadja David M, d'Audigier C, Weiswald L-B, et al. The Wnt antagonist dickkopf-1 increases endothelial progenitor cell angiogenic potential. *Arterioscler Thromb Vasc Biol*. 2010;30:2544-2552.
108. Kestler HA, Kuhl M. Generating a Wnt switch: it's all about the right dosage. *J Cell Biol*. 2011;193:431.

SUPPORTING INFORMATION

Additional Supporting Information may be found online in the Supporting Information section.

How to cite this article: Summers ME, Richmond BW, Menon S, et al. Resident mesenchymal vascular progenitors modulate adaptive angiogenesis and pulmonary remodeling via regulation of canonical Wnt signaling. *The FASEB Journal*. 2020;34:10267–10285. https://doi.org/10.1096/fj.202000629R